Inelastic Electron-Deuteron Scattering and the Rescattering Corrections*

B. Bosco, B. Grossetête, and P. Quarati
Ecole Normale Supérieure, Laboratoire de l'Accélérateur Linéaire, Orsay, France
and
Istituti di Fisica delle Università di Cagliari e Torino, Italy
(Received 29 April 1965)

The inelastic electron-deuteron scattering is completely re-examined on the basis of the recent Orsay experiments described in an accompanying paper. The expression for the differential cross section is derived on a more general basis, the rescattering corrections predicted by different methods are compared extensively, and their effects on the nucleon form factors are discussed.

I. INTRODUCTION

MANY efforts, both experimental[1] and theoretical,[2] have been devoted to the problem of the electrodisintegration of deuterons, with the specific purpose of understanding the neutron form factors. However, the situation is not yet clear in many respects. First, the general problem of treating relativistically the electron-deuteron system has not yet received a satisfactory solution; second, even in the case of a two-body system our knowledge of nuclear forces is still very poor.

The purpose of the present paper is threefold:

(1) To give a new formulation of the general expression for the cross section of inelastic electron-deuteron scattering in terms of nuclear matrix elements and nucleon form factors, which allows a better characterization of the difficulties appearing in the theory.

(2) To present a further analysis of the effect of the interaction of emerging nucleons and a critical comparison with the different methods previously proposed.[3,4] Our approach is the dispersive one proposed by one of the authors[3] and already applied to the S-wave corrections.[2b] In the present analysis this method is extended in order also to include the P-waves of the neutron-proton final-state system. Furthermore, in order to compare our present conclusions with the ones obtained by the model proposed by Durand, in both cases the calculations have been performed for a wide range of momentum transfer.

(3) To interpret on the basis of the above expressed ideas the recent experiments at Orsay.[1d]

Of course, according to Ref. 3, these experiments have been planned in order to determine the S and P waves as carefully as possible. The corrections due to those waves are then introduced in the cross section for deuteron disintegration at the peak, from which the neutron form factors are determined.

Naturally our treatment will be substantially nonrelativistic. Only certain kinematical corrections are introduced automatically and consistently in the theory.

II. FORMULA FOR THE INELASTIC CROSS SECTION

A. General Formulation

The method for deriving the inelastic cross section for the deuteron disintegration is similar to the one for obtaining the elastic cross section already published by one of the authors.[5] The derivation relies on the general properties of electromagnetic vertex functions[6] and on the Sachs interpretation of the nucleon form factors.[7]

The inelastic electron-deuteron scattering will need one more parameter than the corresponding elastic scattering—for example, the energy of the scattered electron. However, once the final energy of the proton-neutron system is given and the total angular momentum and parity relative to the deuteron of this system are determined, then this is equivalent to a two-body system. The corresponding cross section is then obtained by a summation over the angular momenta:

$$\frac{d^2\sigma}{d\Omega dE_3}=\sigma_{\mathrm{Mott}}4M^2\frac{p_r}{E}\frac{1}{3e^2}(1+\epsilon_1)\sum_J\sum_{\lambda_4,\lambda_2}\{(T_{J,\lambda_4,\lambda_2}{}^0)^2$$
$$+(1-\eta)(T_{J,\lambda_4,\lambda_2}{}^+)^2[1+2\tan^2(\theta/2)(1+\epsilon_2)]\}, \quad (1)$$

* Research sponsored in part by the U. S. Air Force Office of Scientific Research OAR through the European Office, Aerospace Research, U. S. Air Force.

[1] a. E. B. Hughes, T. A. Griffy, M. R. Yearian, and R. Hofstadter, in *Proceedings of the International Conference on High Energy Physics, Dubna, 1964* (Atomizdat, Moscow, 1965); b. C. V. Akerloff, K. Berkelman, G. Rouse, and M. Tigner, Phys. Rev. **135**, B810 (1964); c. P. Stein, M. Binkley, R. Mc Allister, B. McDaniel, and W. Woodward, in *Nucleon Structure, Proceedings of The International Conference at Stanford University, 1963*, edited by R. Hofstadter and L. I. Schiff (Stanford University Press, Stanford, California, 1964), p. 373; J. R. Dunning, Jr., K. W. Chen, A. A. Cone, G. Hartwig, N. F. Ramsey, J. K. Walker, and R. Wilson, Phys. Rev. Letters **13**, 631 (1964); d. B. Grossetête, S. Jullian, and P. Lehmann, preceding paper, Phys. Rev. **141**, 1435 (1966).

[2] a. L. Durand, III, in *Nucleon Structure, Proceedings of The International Conference at Stanford University, 1963*, edited by R. Hofstadter and L. I. Schiff (Stanford University Press, Stanford, California, 1964), p. 28; b. B. Bosco and R. B. De Bar, Nuovo Cimento **26**, 604 (1962); c. J. Nuttal and M. L. Whippman, Phys. Rev. **130**, 2495 (1963); d. M. Le Bellac, J. Tran Than Van and F. M. Renard (to be published).

[3] B. Bosco, Nuovo Cimento **23**, 1028 (1961).

[4] L. Durand, III, Phys. Rev. **115**, 1020 (1959).

[5] a. B. Grossetête and P. Lehmann, Nuovo Cimento **28**, 423 (1963); b. B. Grossetête, thesis, Orsay Linear Accelerator Laboratory Report No. LAL.1113 1964 (unpublished); c. B. Grossetête, D. Drickey and P. Lehmann, second preceding paper, Phys. Rev. **141**, 1425 (1966).

[6] L. Durand, III, P. C. De Celles, and R. B. Marr, Phys. Rev. **126**, 1882 (1962).

[7] R. G. Sachs, Phys. Rev. **126**, 2256 (1962).

where

$$\sigma_{\text{Mott}}=\frac{\alpha^2}{4E_1^2}\frac{\cos^2(\theta/2)}{\sin^4(\theta/2)},$$

E_1 is the initial electron energy, E_3 is the final electron energy, E and p_r are, respectively, the energy and the momentum of either of the outgoing nucleons in their center-of-mass system, θ is the scattering angle of the electron, M is the nucleon mass, ϵ_1 equals $-(q^2/8M^2)+2\eta$, ϵ_2 equals $(q^2/4M_D^2)+\frac{1}{2}\xi$, ξ equals $(2E/M_D)^2-1$, and η equals $-\frac{1}{2}\xi^2(q^2/M_D^2)^{-1}(1+q^2/4M_D^2+\frac{1}{2}\xi)^{-1}$, q^2 is the four-momentum transfer, M_D is the deuteron mass, λ_4 and λ_2 are the helicities of the proton-neutron system and of the deuteron, respectively, T^μ are connected to the matrix elements Γ^μ in the Breit frame defined in Ref. 6 by the relation

$$T_{J,\lambda_4,\lambda_2}{}^{\mu}=(2EM_D/p_{02}p_{04})^{1/2}\Gamma_{J,\lambda_4,\lambda_2}{}^{\mu},$$

and p_{02} and p_{04} are the deuteron and the proton-neutron system energies in the Breit frame of reference.

The functions T^μ have a normalization of the states, $1/V$, V being the volume of the system. This allows simpler expressions for the nonrelativistic limits.

Some remarks are now in order concerning Eq. (1):

(1) The functions T^μ depend on two variables. We will choose them as q^2 and p_r.

(2) In Ref. (6) it has been shown that the conservation laws imply that only two components of T^μ are independent; we will choose as independent quantities T^0 and $T^+=(T^1+iT^2)/\sqrt{2}$.

(3) It is evident that Eq. (1) has the general expression

$$\frac{d^2\sigma}{d\Omega dE_3}=\sigma_{\text{Mott}}\left[A(q^2,p_r)+\tan^2\left(\frac{\theta}{2}\right)B(q^2,p_r)\right],$$

which is the well-known consequence of the one-photon exchange approximation.[8]

(4) The structure of Eq. (1) is such that any change in the wave function normalization can be accounted for by a corresponding change in the constant ϵ_1.

(5) The constants η and ϵ_2 are completely determined by the definitions of the charge and magnetic moments of the system.

B. Nonrelativistic Limit

In order to obtain the nonrelativistic limit of the functions T^μ we shall write

$$T_{J,\lambda_4,\lambda_2}{}^{0}=e\int\psi_J{}^{-\lambda_4}(\mathbf{x})[F_c{}^p(q^2)e^{i\mathbf{q}\cdot\mathbf{x}/2}+e^{-i\mathbf{q}\cdot\mathbf{x}/2}F_c{}^n(q^2)]\times\psi_d{}^{\lambda_2}(\mathbf{x})d^3x,$$

$$\mathbf{T}_{J,\lambda_4,\lambda_2}=\frac{ie}{2M}\int\psi_J{}^{-\lambda_4}(\mathbf{x})[\mathbf{q}\times\boldsymbol{\sigma}_p\mu_pF_m{}^p(q^2)e^{i\mathbf{q}\cdot\mathbf{x}/2}+\mathbf{q}\times\boldsymbol{\sigma}_n\mu_nF_m{}^n(q^2)e^{-i\mathbf{q}\cdot\mathbf{x}/2}]\psi_d{}^{\lambda_2}(\mathbf{x})d^3x, \quad (2)$$

where $\psi_J{}^{-\lambda_4}(\mathbf{x})$ is the nonrelativistic wave function of the neutron-proton system with total angular momentum J and $J_z=-\lambda_4$, normalized to the asymptotic condition

$$\psi_{JLS}\underset{t\to\infty}{\longrightarrow}(p_rr)^{-1}\sin(p_rr-\tfrac{1}{2}L\pi+\delta_{JLS}),$$

$\psi_d(\mathbf{x})$ is the deuteron wave function, $F_c{}^p$, $F_c{}^n$, $F_m{}^p$, $F_m{}^n$ are the Sachs form factors, and μ_p and μ_n are the total magnetic moments of the proton and neutron, respectively.

Equations (2) are the obvious generalization to the inelastic processes of the expressions which can be written in the elastic case.[5c]

Equations (2) are nonrelativistic expressions which cannot be written without any ambiguity in particular in the normalization of the wave functions. We follow the Sachs interpretation of the form factors and so we have not placed a contraction term in the wave functions. In fact, as outlined by Nuttal and Whippman[2c] the problem is not clear. Equations (2) are only Fourier transforms of an electromagnetic distribution and slightly different from the matrix elements given by Foldy-Wouthuysen transformation. For example, if we use the Sachs nucleon form factors, T_0 differs from the expression given by Durand,[9] by $(1+q^2/8M^2)$. Gourdin[10] has observed a little inconsistency in Ref. 7 and defined other nuclear charge and magnetic form factors which are the Sachs form factors divided by $[1+(q^2/4M^2)]^{1/2}$. Introducing those form factors, only negligible differences subsist between the two approaches and we obtain the same T_0 expression as Durand.[9]

In writing the nonrelativistic expression for the current the orbital term has been neglected. This is because we neglect the coupling between waves with different angular momenta. The resulting expression for the differential cross section is then

$$\frac{d^2\sigma}{d\Omega dE_3}=\sigma_{\text{Mott}}\frac{M^2}{\pi}\frac{p_r}{E}(1+\epsilon_1)I(\theta,q^2), \quad (3)$$

and

$$I(\theta,q^2)=\tfrac{1}{3}\sum_J\sum_L(2J+1)K_{J,L,1}{}^2(F_c{}^p+(-1)^LF_c{}^n)^2\times\frac{1}{3}\frac{q^2}{4M^2}(1-\eta)[1+2(1+\epsilon_2)\tan^2(\theta/2)]\times\sum_L\{\tfrac{1}{2}(\mu_pF_m{}^p+(-1)^L\mu_nF_m{}^n)^2[(3L+4)K_{L+1,L,1}{}^2+(2L-1)K_{L,L,1}{}^2+(3L-1)K_{L-1,L,1}{}^2]+[\mu_pF_m{}^p-(-1)^L\mu_nF_m{}^n]^2(2L+1)K_{L,L,0}{}^2\}, \quad (4)$$

where

$$K_{J,L,S}=\frac{1}{p_r}\int_0^\infty F_{JLS}(p_r,r)J_L(\tfrac{1}{2}qr)u(r)dr \quad (5)$$

are defined according to Durand's paper.[9]

[8] M. Gourdin, Nuovo Cimento **21**, 1094 (1961).

[9] L. Durand, III, Phys. Rev. **123**, 1393 (1961).

[10] M. Gourdin, Nuovo Cimento **36**, 129 (1965).

III. FREE SOLUTIONS RESULTS

If the proton-neutron system is described by plane waves the summation can be performed in Eq. (4) and one obtains[5b]

$$I(\theta,q^2)=[(F_c{}^p)^2+(F_c{}^n)^2]M(p_r,q)+2F_c{}^pF_c{}^nN(p_r,q)$$
$$+\frac{q^2}{4M^2}(1-\eta)[1+(1+\epsilon_2)2\tan^2(\theta/2)]$$
$$\times\{[(\mu_pF_m{}^p)^2+(\mu_nF_m{}^n)^2]M(p_r,q)$$
$$+\tfrac{2}{3}\mu_pF_m{}^p\mu_nF_m{}^nN(p_r,q)\}, \quad (6)$$

with $M(p_r,q)$ and $N(p_r,q)$ defined as in Ref. 9.

On the basis of Eq. (6), we can derive a simplified expression of $I(\theta,q^2)$ to be valid at the peak, in which the terms proportional to $F_c{}^pF_c{}^n$ and to $F_m{}^pF_m{}^n$ are neglected. It has been found[5b] that at low q^2 the contribution due to these terms may be quite relevant. In Table I corrections due to this term for different values of q^2 are reported.

Finally in Fig. 1 the results predicted by Eq. (6) are compared with the experimental results[1d] for the whole spectrum. As easily observed, above the threshold the experiments give cross sections greater than the ones predicted by Eq. (6).

IV. RESCATTERING CORRECTIONS

Many attempts have been made to evaluate the rescattering corrections.[2c,3,9] Substantially they have been evaluated by two different methods which we shall outline here. The first one assumes a potential, from which wave functions are computed by solving the corresponding Schrödinger equation and then evaluating the matrix elements. The second one relies on the analytic properties of the matrix elements.[11] These properties together with elastic unitarity allow an Omnes integral equation to be written for each matrix element, in terms of the corresponding Born approximation (free-wave solution) and the phase shifts of the elastic scattering of the outgoing nucleons.

Both methods are of course affected by difficulties; the difficulty of the potential method is obvious, since we know only the asymptotic part of the potential between the nucleons and therefore the method relies on models which may give very different answers. The second method needs the introduction of constants which are determined directly by the experiments, in order to account for the discontinuities due to the anomalous thresholds.

TABLE I. Percentage of the terms in $F_m{}^n\,F_m{}^p$ in the magnetic term of the cross sections at the quasi-elastic peak.

q^2 (F^{-2})	0.7	0.9	1.5	2.0	2.5	3.4	5.0	7.0	9.1
Percentage of the terms in $F_m{}^n\,F_m{}^p$	9.4	7.4	4.6	3.2	2.4	1.6	0.8	0.5	0.4

[11] B. Bosco, Phys. Rev. **123**, 1072 (1961).

It has been stated[2a] that the two methods are equivalent. While this is certainly true from a theoretical point of view since both methods are different expressions of the Schrödinger mechanism, there is no reason that the practical results of the two methods should be identical. Indeed, we do not know the potential which generates the experimental phase shifts we use in the dispersive approach or the phenomenological constants we determine from the experiments.

A simplified version of the potential method has been presented by Durand[9] in order to avoid the lengthy computer calculations. We applied this method very widely. We shall discuss this version in the next subsection, while in the subsequent one we shall discuss the dispersive approach. In the following calculation the phase shifts plotted in Fig. 2 will be used. A third very simple model is explained in the Appendix.

A. The Durand Model

This method has been presented first by Durand[9] and applied by him in very particular cases. Even if we suspect its validity, particularly near the threshold, (because of the singlet S state and the proximity of the deuteron pole term), it seems very interesting to extend this very simple method and to compare it with the experiment. In fact, we find this approximation somewhat in agreement with the experiment.

Such a simple model can be useful in some applications where one needs an expression of the theoretical cross section, e.g., for calculating the radiative corrections along the complete spectra.[1d] We apply this method under very different conditions. We even calculate final-state corrections for very high q^2 and we find acceptable results. Then this method can be used to give qualitative indications on the behavior of the cross section under the variation of some parameters, bearing in mind that this model cannot be an exact representation of a complex problem.

Durand has treated the problem assuming a square well potential of fixed range $r_0=2$ F. Outside this range he uses the asymptotic wave functions with experimentally determined phase shifts. The continuity of the wave functions and their first derivatives at r_0 should determine the depths of the potentials. However, since the resulting transcendental equations have an infinite number of solutions, a further condition is needed in order to completely define the potential.

A supplementary condition has been imposed by selecting the minimum absolute value for the potential depth.[12]

[12] We select the solution which corresponds to the minimum absolute value for the depth of the potential. In some exceptional cases, the depth corresponding to this solution is very important. (The maximum is 220 MeV for S waves, 340 MeV for P waves, 500 MeV for D waves). This model introduces very apparent discontinuities (Figs. 3 and 4).

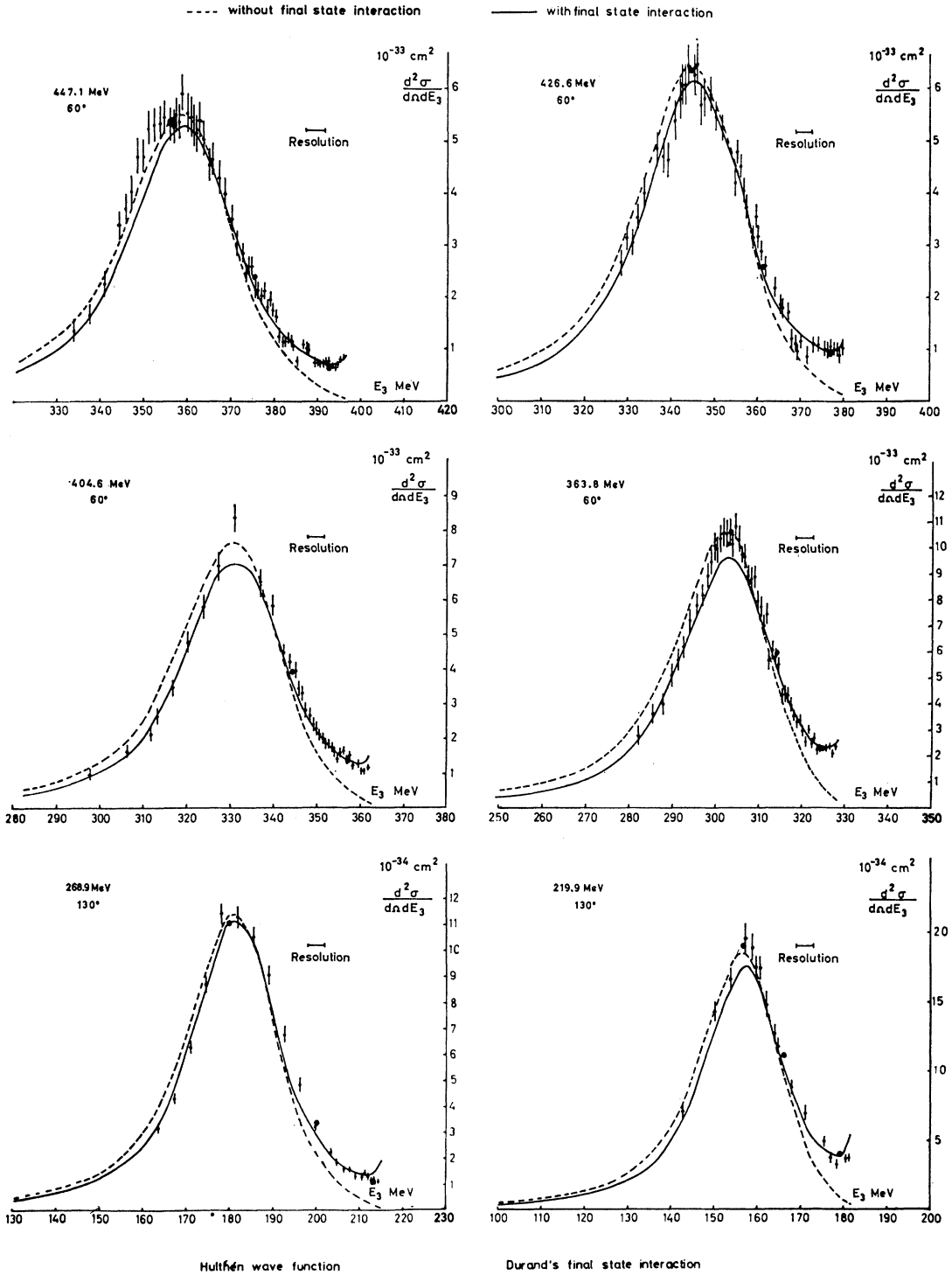

FIG. 1. The spectra predicted by the Durand model compared to the experimental ones. The dashed line is obtained neglecting the final-state interaction; the solid line includes the final-state interaction. The bound state is described by a Hulthén wave function.

In order to compare with the experimental data the calculation has been performed for a wide range of q^2.

In Fig. 3 the quantities

$$D_{JLS}=(K_{JLS}^2-K_L^2)/K_L^2,$$

where K_L are the matrix elements (5) computed with free waves, are plotted versus q^2, at the quasi-elastic peak. In Fig. 4 the corresponding quantities

$$\Delta I=\frac{I(\theta,q^2)-I_0(\theta,q^2)}{I_0(\theta,q^2)}$$

are plotted versus q^2 at $\theta=60°$ and 130°. $I_0(\theta,q^2)$ is the function $I(\theta,q^2)$ computed with free waves and $I(\theta,q^2)$ includes the final interactions in the S, P, D waves. One can easily observe that such corrections are of the order of 1.5% for q^2 above 7.5 F^{-2}.

The comparison with the experimental data for the whole spectrum is given in Figs. 1 and 5. The calculations have been performed for two different deuteron wave functions: a Hulthén wave function and a wave function with a hard core. A noticeable disagreement with the experiments is evident from these figures between the threshold and the peak.

B. Dispersive Approach

We shall devote this subsection to the dispersive treatment of the rescattering corrections. Since the theoretical formula and hypothesis have already been published in a number of papers,[11,3,2b] we shall only recall the explicit expressions we need for the purpose of the present calculations. We wish to compute the corrections for S and P waves. Let us first define the matrix elements which are convenient for the dispersive treatment. We shall introduce

$$S_q{}^{\mu}(p_r)=q\int_0^{\infty}\psi_{\mu}{}^{\text{out}*}(p_r,r)j_0(\tfrac{1}{2}qr)u(r)\,dr, \qquad (7)$$

$${}^{\mu}P_q{}^{\nu}(p_r)=q^2\int_0^{\infty}\psi_{\mu\nu}{}^{\text{out}*}(p_r,r)j_1(\tfrac{1}{2}qr)u(r)\,dr. \qquad (8)$$

$\psi_{\mu}{}^{\text{out}}$ is the outgoing function for the s waves which may belong to the singlet ($\mu=0$) or triplet ($\mu=1$) state. It is normalized to the asymptotic behavior

$$\psi_{\mu}{}^{\text{out}}\underset{r\to\infty}{\longrightarrow}[\sin(p_r r+\delta_{\mu})]e^{i\delta_{\mu}}.$$

$\psi_{\mu\nu}{}^{\text{out}}$ is the outgoing wave function for the P waves and may belong to four different states according to the spin μ and the total angular momentum ν of the state. It is normalized to the asymptotic behavior

$$\psi_{\mu z}{}^{\text{out}}\underset{r\to\infty}{\longrightarrow}\frac{1}{p_r r}[\sin(p_r r-\tfrac{1}{2}\pi+\delta_{\nu 1\mu})]e^{i\delta_{\nu 1\mu}}.$$

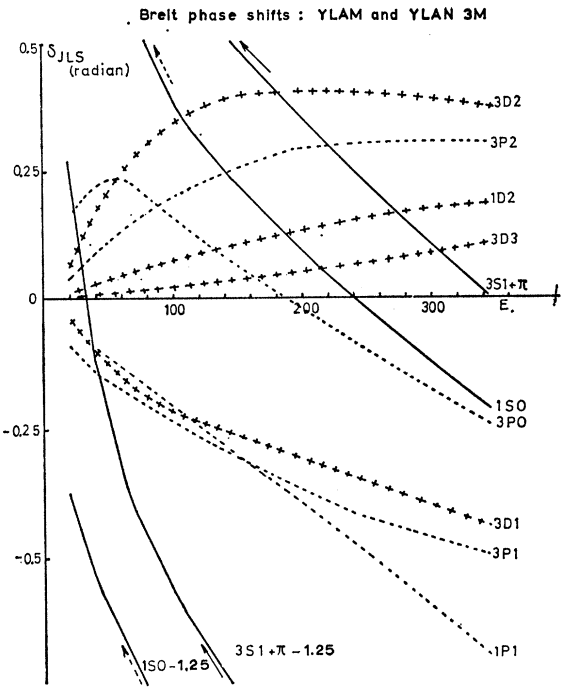

FIG. 2. The sets of phase shifts utilized in the calculations. They are the YLAM and YLAN3M published by Breit.

The quantities $S_q{}^{\mu}(p_r)$ and ${}^{\mu}P_q{}^{\nu}(p_r)$ are defined in such a way to be dimensionless. They are related to the matrix elements (5) by the relations

$$S_q{}^{\mu}(p_r)=p_r q K_{\mu 0\mu},$$
$${}^{u}P_q{}^{\nu}(p_r)=q^2K_{\nu 1\mu}. \qquad (9)$$

Applying the usual dispersive techniques[11] one is led to the following expressions for the quantities (7) and (8):

$$S_q{}^{\mu}(E_r)=\left\{\left[A_{\mu}+B_q{}^{s}(E)+\frac{\Gamma(q)}{E+\alpha^2}\delta_{\mu 1}\right]\cos\delta_{\mu}\right.$$
$$+\frac{1}{\pi}e^{\rho_{\mu}(E_r)}E_r^{1/2}P\int_0^{\infty}\frac{1}{E'^{1/2}}$$
$$\times\left[A_{\mu}+B_q{}^{s}(E_r')+\frac{\Gamma(q)E_r'^{1,2}}{E_r'+\alpha^2}\delta_{\mu 1}\right]$$
$$\left.\times\frac{e^{-\rho_{\mu}(E_r')}\sin\delta_{\mu}(E')\,dE_r'}{E_r'-E_r}\right\}e^{i\delta_{\mu}}; \qquad (7')$$

$${}^{\mu}P_q{}^{\nu}(E_r)=\left\{[A_{\mu\nu}+B_q{}^{p}(E)]\cos\delta_{\nu 1\mu}\right.$$
$$+\frac{1}{\pi}e^{\rho_{\mu\nu}(E)}E_r^{1/2}P\int_0^{\infty}\frac{A_{\mu\nu}+B_q{}^{p}(E_r')}{E_r'^{1/2}(E_r'-E_r)}$$
$$\left.\times e^{-\rho_{\mu\nu}(E_r')}\sin\delta_{\nu 1\mu}dE_r'\right\}e^{i\delta_{\nu 1\mu}}. \qquad (8')$$

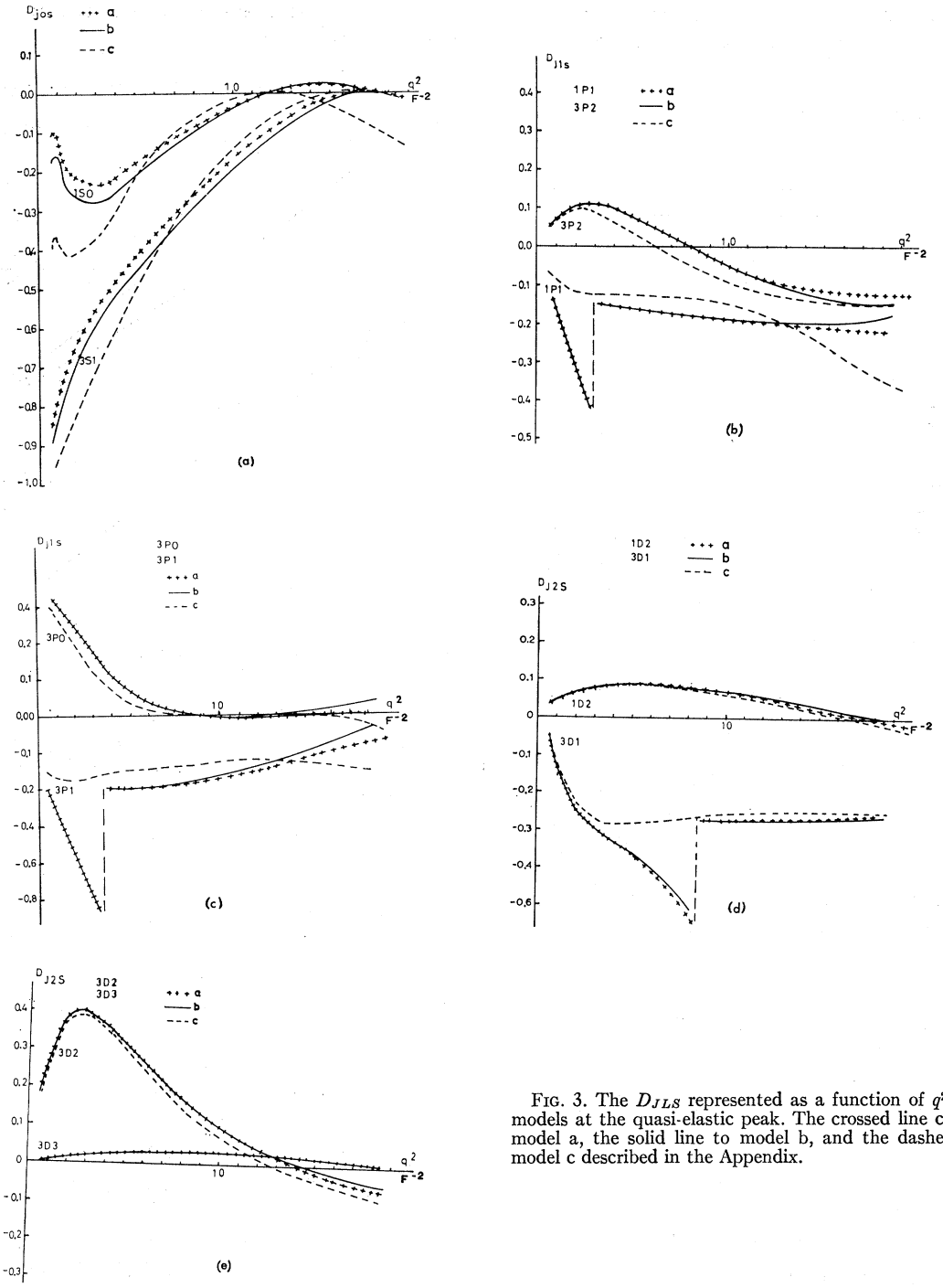

FIG. 3. The D_{JLS} represented as a function of q^2 for different models at the quasi-elastic peak. The crossed line corresponds to model a, the solid line to model b, and the dashed line to the model c described in the Appendix.

A_μ, $A_{\mu\nu}$ are constants which must be determined by the experiments.

$$B_q{}^s(E_r)=-\frac{1}{2}\left\{\ln\frac{\alpha^2+(E_r{}^{1/2}+\frac{1}{2}q)^2}{\alpha^2+(E_r{}^{1/2}-\frac{1}{2}q)^2}-\ln\frac{\beta^2+(E_r{}^{1/2}+\frac{1}{2}q)^2}{\beta^2+(E_r{}^{1/2}-\frac{1}{2}q)^2}\right\}$$

is the solution for $S_q{}^\mu(E_r)$ in the free-wave approximation.

$$B_q{}^p(E_r)=\frac{1}{2E_r}\left\{\alpha^2+E_r+(\tfrac{1}{2}q)^2\ln\frac{\alpha^2+(E_r{}^{1/2}+\frac{1}{2}q)^2}{\alpha^2+(E_r{}^{1/2}-\frac{1}{2}q)^2}\right.$$
$$\left.-\beta^2+E_r+(\tfrac{1}{2}q)^2\ln\frac{\beta^2+(E_r{}^{1,2}+\frac{1}{2}q)^2}{\beta^2+(E_r{}^{1/2}-\frac{1}{2}q)^2}\right\}$$

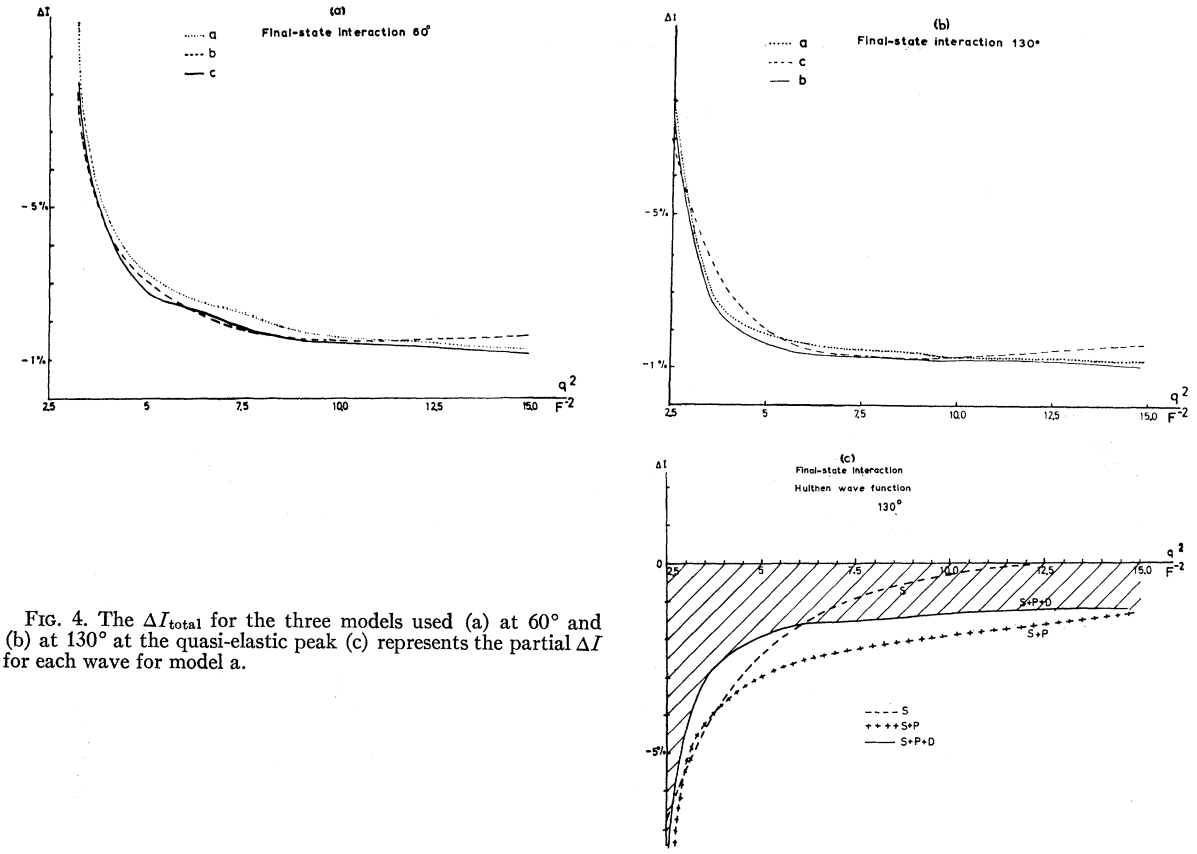

FIG. 4. The ΔI_{total} for the three models used (a) at 60° and (b) at 130° at the quasi-elastic peak (c) represents the partial ΔI for each wave for model a.

is the analogous solution for ${}^{\mu}P_{q}{}^{\nu}(E_r)$.

$$\Gamma(q)=-\frac{4\alpha}{1-\alpha r_0}\left\{\arctan\frac{q}{4\alpha}+\arctan\frac{q}{4\beta}-2\arctan\frac{q}{2(\alpha+\beta)}\right\}$$

TABLE II. Percentage of the S, P, and D waves near the most accurate points taken in the experiments at Orsay.

E_1 (MeV)	θ (deg)	E_3 (MeV)	q^2 F^{-2}	Percentage of the waves $\%S$	$\%P$	$\%D$	% other waves
447.1	60	392.3	4.51	71.5	25.4	2.7	0.5
		376.8	4.33	29.1	38.8	15.6	16.6
		357.0	4.10	14.0	27.8	16.7	41.3
426.6	60	377.0	4.13	75.2	22.6	1.9	0.3
		362.8	3.98	31.7	39.2	14.8	14.3
		345.4	3.79	15.5	28.8	17.0	38.7
404.6	60	357.2	3.71	63.9	30.1	4.6	1.4
		344.9	3.59	29.5	37.8	15.5	17.2
		332.4	3.46	17.3	30.1	17.3	35.3
363.8	60	325.6	3.04	72.1	24.3	2.8	0.8
		313.6	2.93	30.9	36.7	15.5	16.9
		303.5	2.84	20.2	31.7	17.5	30.6
268.9	130	212.8	4.83	76.5	22.2	1.2	0.1
		199.4	4.53	30.3	45.4	12.3	12.0
		181.4	4.12	12.5	31.1	14.5	41.9
219.9	130	179.5	3.33	72.9	24.9	1.6	0.7
		165.5	3.07	23.5	40.2	14.2	22.2
		156.2	2.90	16.7	35.0	15.1	33.2

is the residue of the bound state and appears only in triplet solution. Therefore this term is multiplied by the Kronecker symbol $\delta_{\mu 1}$. $\alpha=(MB)^{1/2}$, B being the binding energy of the deuteron; δ_{μ} and $\delta_{\nu 1\mu}$ are the phase shifts for S and P waves, respectively; E_r is the relative energy of the outgoing particles. The ρ are defined by means of the phase shifts through the relation

$$\rho(E_r)=\frac{1}{\pi}P\int_0^{\infty}\frac{\delta(E_r')}{E_r'-E_r}dE_r'.$$

The cross section can thus be described by means of six constants, one for each wave (${}^3S_1$, ${}^1S_0$, ${}^3P_0$, ${}^3P_1$, ${}^3P_2$, ${}^1P_1$):

$$\frac{d^2\sigma}{d\Omega dE_3}=\sum_{S,P\text{ waves}}[A^2f_1(\theta,q,p_r)+Af_2(\theta,q,p_r)+f_3(\theta,q,p_r)]+\frac{d^2\sigma}{d\Omega dE_3}\quad\text{(Born approx. of all the remaining waves)},\quad(10)$$

TABLE III. Constants of the dispersive approach obtained using the experimental data of Orsay.

${}^3S_1$	${}^1S_0$	${}^3P_0$	${}^3P_1$	${}^3P_2$	${}^1P_1$
−0.020	0.100	1.200	−0.950	0.450	2.300

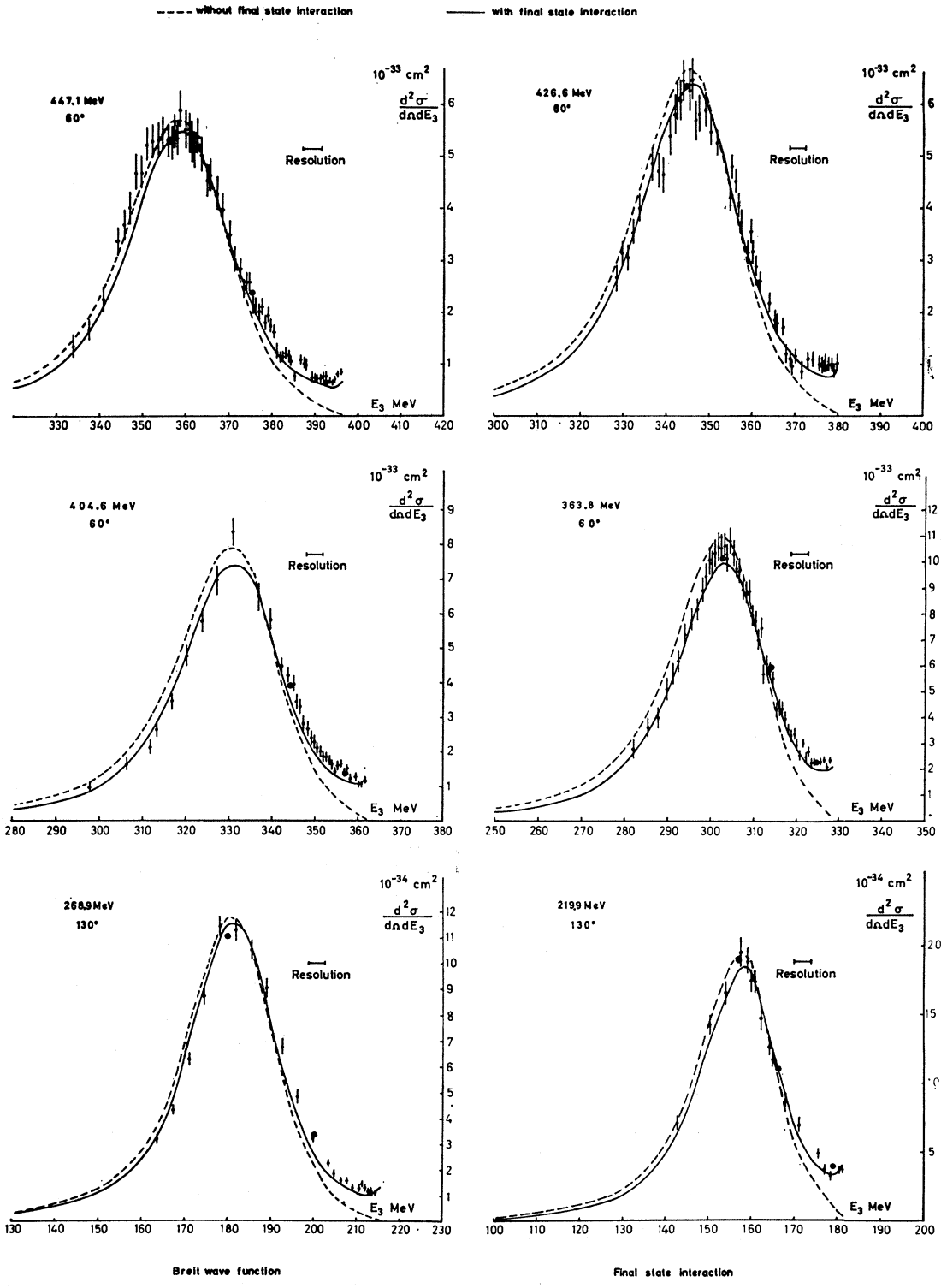

FIG. 5. The comparison of model b with the experimental spectra (solid line). The dashed line is obtained by neglecting the interaction in the final state.

where the A and f_i are different for each wave. The explicit expressions for the f_i can easily be derived by inserting Eqs. (7′) and (8′) in Eqs. (3) and (4) and by identifying the result with Eq. (10). We shall not write them here.

We use the Orsay experimental results to determine these constants.[1d] We first determined the two constants for the S waves. To this purpose the experimental cross sections corresponding to kinematical situations in which the S waves are dominant have been utilized (see Table II). All other waves have been accounted for in Born approximation.

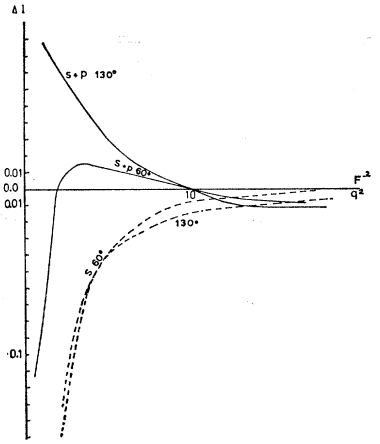

FIG. 6. The quantities ΔI predicted by the dispersive approach for 60° and 130° at the quasi-elastic peak. The dashed lines represent the ΔI_s, the solid lines represent ΔI_{s+p}.

TABLE IV. ΔI for each wave and total ΔI calculated with different theories near the experimental points of Orsay. (See Appendix.)

E_1 (MeV)	θ (deg)	E_3 (MeV)	ΔI_S	ΔI_P	ΔI_D	ΔI_{total}	Theories
				Threshold			
447.1	60	392.3	2.364	0.107	0.056	2.527	a
			2.285	0.139	0.075	2.498	b
			0.237	0.122	0.074	0.434	c
			1.959	0.551	···	2.511	Dispersive
426.6	60	377.0	2.886	0.085	0.038	3.009	a
			2.810	0.109	0.050	2.968	b
			0.379	0.097	0.050	0.526	c
			2.419	0.526	···	2.945	Dispersive
404.6	60	357.2	1.332	0.062	0.046	1.440	a
			1.234	0.076	0.056	1.365	b
			0.132	0.083	0.056	0.269	c
			1.132	0.456	···	1.588	Dispersive
363.8	60	325.6	1.866	0.037	0.021	1.924	a
			1.745	0.045	0.025	1.814	b
			0.290	0.049	0.025	0.364	c
			1.670	0.420	···	2.091	Dispersive
268.9	130	212.8	5.034	0.150	0.031	5.214	a
			4.936	0.203	0.043	5.182	b
			0.875	0.165	0.042	1.082	c
			3.300	0.797	···	4.097	Dispersive
219.9	130	179.5	3.590	0.062	0.016	3.668	a
			3.396	0.076	0.019	3.491	b
			1.037	0.078	0.019	1.134	c
			2.540	0.627	···	3.167	Dispersive
				P waves			
447.1	60	376.8	0.077	0.000	0.058	0.136	a
			0.063	0.005	0.063	0.131	b
			−0.028	0.045	0.063	0.080	c
			0.053	0.231	···	0.284	Dispersive
426.6	60	362.8	0.095	0.007	0.055	0.157	a
			0.077	0.011	0.060	0.149	b
			−0.037	0.047	0.060	0.071	c
			0.065	0.243	···	0.309	Dispersive
404.6	60	344.9	0.045	0.001	0.045	0.091	a
			0.032	0.005	0.048	0.086	b
			−0.057	0.036	0.048	0.028	c
			0.021	0.212	···	0.233	Dispersive
363.8	60	313.6	0.009	0.002	0.035	0.046	a
			−0.002	0.005	0.037	0.040	b
			−0.091	0.028	0.037	−0.026	c
			−0.051	0.201	···	0.186	Dispersive
268.9	130	199.4	0.176	0.015	0.047	0.238	a
			0.147	0.022	0.022	0.221	b
			0.027	0.071	0.052	0.150	c
			0.065	0.364	···	0.429	Dispersive
219.9	130	165.5	0.020	−0.007	0.024	0.038	a
			0.011	−0.003	0.025	0.033	b
			−0.041	0.028	0.025	0.012	c
			−0.031	0.232	···	0.201	Dispersive

TABLE IV (*continued*).

E_1 (MeV)	θ (deg)	E_3 (MeV)	ΔI_S	ΔI_P	ΔI_D	ΔI_{total}	Theories
				Peak			
447.1	60	357.0	−0.058	−0.004	0.009	−0.053	a
			−0.052	−0.004	0.009	−0.047	b
			−0.059	−0.007	0.010	−0.056	c
			−0.059	0.063	···	0.004	Dispersive
426.6	60	345.4	−0.062	0.001	0.012	−0.049	a
			−0.056	0.000	0.012	−0.043	b
			−0.064	−0.003	0.013	−0.054	c
			−0.064	0.074	···	0.011	Dispersive
404.6	60	332.4	−0.067	−0.025	0.016	−0.075	a
			−0.061	−0.022	0.016	−0.068	b
			−0.075	−0.002	0.016	−0.058	c
			−0.069	0.089	···	0.020	Dispersive
363.8	60	303.5	−0.090	−0.019	0.016	−0.093	a
			−0.084	−0.017	0.016	−0.085	b
			−0.104	0.004	0.016	−0.084	c
			−0.096	0.108	···	0.011	Dispersive
268.9	130	181.4	−0.033	−0.001	0.011	−0.022	a
			−0.030	−0.001	0.012	−0.020	b
			−0.035	−0.005	0.012	−0.028	c
			−0.052	0.089	···	0.037	Dispersive
219.9	130	156.2	−0.059	−0.024	0.011	−0.072	a
			−0.055	−0.022	0.011	−0.066	b
			−0.068	0.000	0.011	−0.057	c
			−0.080	0.134	···	0.055	Dispersive

In this case Eq. (10) takes the form

$$\frac{d^2\sigma}{d\Omega dE_3}=\sum_{S\text{ waves}}[A^2f_1+Af_2+f_3]+\frac{d^2\sigma}{d\Omega dE_3}\ \text{(Born approx. of all the remaining waves)}. \quad (11)$$

Equation (11) furnishes a system of two equations of second order in the two unknown constants A_μ which can easily be solved by numerical methods. Of the four solutions only one is constant with respect to the momentum transfer.[13]

With this solution we proceed to determine the constants for the P waves. We utilize the experimental cross sections with the highest possible contributions from P waves (see Table II). Equation (10) furnishes a system of four equations of second order in the four unknown constants $A_{\mu\nu}$ for the P waves. Also in this case a solution satisfying all the requirements is found.

A final check is made on the spectrum in order to redetermine the constants for the S waves.

The resulting procedure is a rapidly convergent one. The final values of the constants are reported in Table III. With these constants the predicted values of

$$\Delta I=\frac{I(\theta,q^2)-I_0(\theta,q^2)}{I_0(\theta,q^2)},$$

for $\theta=60°$ and $130°$ are plotted versus q^2 in Fig. 6. The

TABLE V. Comparison of the experimental cross sections with the theoretical ones for different hypothesis. (See Appendix).

E_1 (MeV)	θ (deg)	E_3 (MeV)	$\left(\frac{d^2\sigma}{d\Omega dE_3}\right)_{\text{expt}}$ (10^{-33} cm^2)	$\frac{d^2\sigma}{d\Omega dE_3}$ Dispersive	$\frac{d^2\sigma}{d\Omega dE_3}$ a	$\frac{d^2\sigma}{d\Omega dE_3}$ b	$\frac{d^2\sigma}{d\Omega dE_3}$ c
447.1	60	392.7	0.651 ±0.033	0.717	0.728	0.570	0.203
		375.7	2.392 ±0.095	2.304	2.131	2.063	1.998
426.6	60	377.2	0.918 ±0.046	0.937	0.966	0.767	0.257
		361.9	2.576 ±0.100	2.697	2.419	2.372	2.243
404.6	60	357.0	1.387 ±0.062	1.303	1.393	1.161	0.643
		344.6	3.928 ±0.149	3.814	3.458	3.439	3.270
363.8	60	325.3	2.298 ±0.057	2.356	2.303	1.970	0.988
		314.2	5.982 ±0.215	5.806	5.266	5.262	4.878
268.9	130	212.9	0.1139±0.0056	0.1153	0.1454	0.1082	0.0358
		200.1	0.3341±0.0107	0.3182	0.2711	0.2525	0.2346
219.9	130	179.2	0.3995±0.0168	0.3594	0.4095	0.3400	0.1690
		166.7	1.117 ±0.039	1.157	1.025	1.034	1.001

[13] With this solution the matrix elements for S waves have the sign of the free-wave solutions.

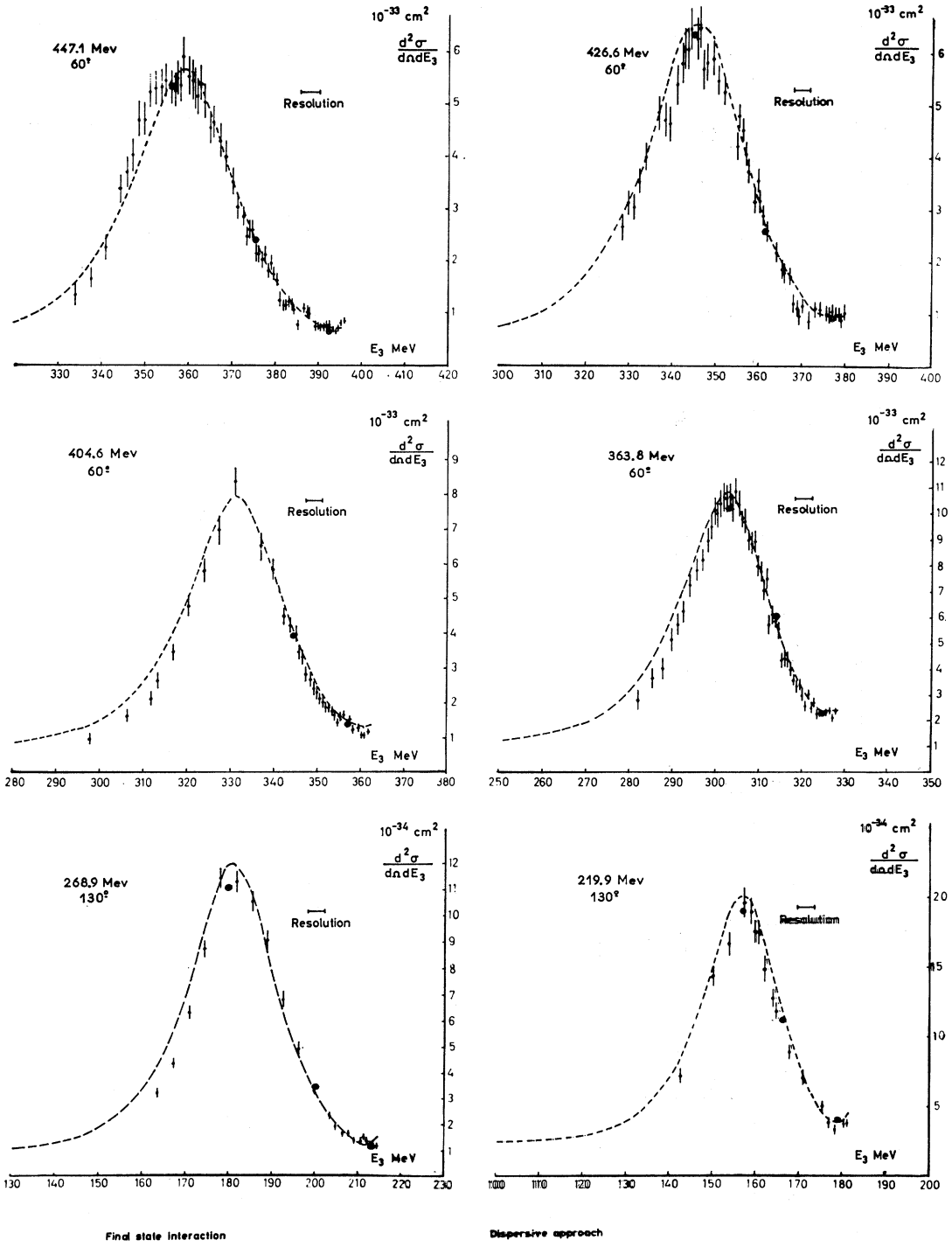

FIG. 7. The spectra predicted by the dispersive approach compared to the experimental ones. The bound state is described by a Hulthén wave function.

comparison with the experimental data for the whole spectrum is given in Fig. 7. A better agreement is obtained for all the spectra in all the kinematical situations considered.

V. CONCLUSIONS AND NUMERICAL RESULTS

We wish to summarize in this section the main conclusions we can draw from the preceding analysis and to present more detailed numerical results. A first

TABLE VI. Comparison of the cross sections at the quasi-elastic peak taken at Orsay, with the theoretical ones supposing $F_m^n = F_m^p$ and $F_c^n = 0$. $\sigma_{\text{Durand simple}}$ is the simple formula given by Durand (Ref. 9) and valid at the quasi-elastic peak. (See Appendix.)

E_1 (MeV)	θ (deg)	q^2 (F^{-2})	E_3 (MeV)	$\left(\frac{d^2\sigma}{d\Omega dE_3}\right)_{\text{expt}}$ (10^{-33} cm^2)	F_p^2	Without final-state interactions			With final-state interactions			
						σ Durand (simple)	σ Durand Hulthén	σ Durand Breit	σ Durand a	σ Durand b	σ Durand c	σ Disper.
447.1	60	4.099	356.8	5.30 ±0.20	0.441	5.23	5.20	5.37	4.91	5.12	5.09	5.24
426.6	60	3.786	345.3	6.33 ±0.25	0.467	6.13	6.30	6.53	5.98	6.25	6.17	6.35
363.8	60	2.829	302.6	10.11 ±0.35	0.537	10.07	10.22	10.60	9.20	9.63	9.67	10.29
268.9	130	4.089	180.1	1.109±0.34	0.445	1.108	1.097	1.141	1.066	1.111	1.104	1.144
219.9	130	2.908	157.3	1.905±0.65	0.545	1.842	1.846	1.923	1.730	1.813	1.824	1.960

TABLE VII. The resulting neutron from factors under the different hypotheses on the bound-state wave function and final-state interactions. (See Appendix.)

q^2	$(F_c^n/F_c^p)^2$								F_m^n/F_m^p							
	Durand (simple)	Hulthén without inter-action	Breit without inter-action	a	b	c	Disper.	Error	Durand (simple)	Hulthén without inter-action	Breit without inter-action	a	b	c	Disper.	Error
2.85	−0.024	−0.048	−0.083	0.092	0.047	0.044	−0.008	±0.071	1.076	1.083	1.017	1.136	1.074	1.066	0.947	±0.082
4.1	0.026	0.028	0.007	0.117	0.078	0.082	0.062	±0.080	0.994	1.012	0.944	1.037	0.976	0.985	0.925	±0.068

observation concerns the percentage of the different waves. The region below the quasi-elastic peak is clearly dominated by the first few S, P, and D (see Table II).

At the quasi-elastic peak the percentage of the other waves is certainly comparable to that of the waves we have corrected. However, we neglect these conditions since the phase shifts corresponding to the higher waves are small and the relative energy of the outgoing particles is high enough to make these interactions less important.

The effects of the corrections for each wave on the differential cross section for various potential models and for the dispersive approach corresponding to many experimental points are presented in Table IV.

A more detailed comparison between the predictions of the different approaches discussed in the preceding sections and the experimental cross sections is given in Table V. It is possible to obtain a consistent agreement with the experiments with the dispersive treatment. The other models present a poorer agreement. Of course this is due to the fact that the constants appearing in the first method have been determined in the region below the peak. However, we wish to point out that the agreement is maintained over the whole spectrum.

From Table IV one may observe that the good agreement of the dispersive approach is obtained by a considerable enchacement of the P-wave corrections. The region of momentum transfer we have chosen (q^2 between 2.8 and 4.1 F^{-2}) is particularly sensitive to the final-state interaction. This is the reason why we concentrated on it.

In Table VI the cross sections, according to formulas (3) and (4), without and with rescattering corrections computed with different models, are given in the hypothesis $F_c^n=0$, $F_m^p=F_m^n$.

Finally, in Table VII the quantities $(F_c^n/F_c^p)^2$ and F_m^n/F_m^p are reported for each model. It is interesting to notice that also here at the peak, the rescattering corrections obtained by the dispersive approach are working in the opposite direction to the potential models. Furthermore the form factors are very sensitive to these corrections. Unfortunately the accuracy of the present experimental data is still not sufficient for a definite determination of the form factors at relatively small momentum transfers.

At higher momentum transfers all approaches show that in the peak region the corrections are negligible.

ACKNOWLEDGMENTS

We want to thank Professor P. Lehmann for his constant interest in this work and very useful discussions. We are indebted to Dr. J. Tran Than Van for a part of a numerical program. Two of us (B.B and P.Q.) wish to thank Professor G. R. Bishop for having originated this collaboration, Professor S. Fubini for the encouragement and the financial support which has made possible this collaboration, and Professor A. Blanc-Lapierre for the kind hospitality received in his Laboratory.

APPENDIX

Different models used in the potential approach:

The model a is obtained by describing the bound state by a Hulthén wave function and the final-state interaction by the Durand method.

The model b has the bound state described by a Breit wave function with repulsive core of 0.5 F. Only the S part of this wave function has been considered and this part has been normalized to 1. The final wave function is the same of the model a.

In model c the wave function of the bound state is the same as the model b. The final wave function is the one described by de Swart and Marshak[14] for the photodisintegration process. In this function the asymptotic behavior is utilized from 1.5 F to infinity; below this distance only the regular part is retained.

[14] J. J. De Swart and R. E. Marshak, Phys. Rev. **111**, 272 (1958).